RSC Advances

PAPER

Cite this: *RSC Adv.*, 2020, **10**, 23749

Preparation of high-performance toluene adsorbents by sugarcane bagasse carbonization combined with surface modification†

Yu Wang,[a] Wangsheng Chen,[b] Bo Zhao,*[a] Huaqin Wang,[a] Linbo Qin[a] and Jun Han*[ab]

A series of activated carbons were prepared by carbonizing sugarcane bagasse combined with surface modification, which showed an excellent performance of adsorbing toluene (522 mg g^{-1} at 30 °C). The results demonstrated that the enhancement of the activated temperature was benefit to promote the porosity and specific surface area (BET) of ACs. Thus, AC-800 showed optimal adsorption and its toluene adsorption performance was better than that of most ACs in the literature. Five consecutive adsorption–desorption cycles presented that AC-800's toluene adsorptive capacity was as high as 522 mg g^{-1} (30 °C), and toluene adsorptive capacity was only decreased by 4.5%. According to the fraction of N-containing functional groups and the binding energy of toluene on N-containing functional groups, pyridinic-N (N-6) was believed to contribute more to toluene adsorption. Moreover, the Bangham model was considered as the best model of describing toluene adsorption on AC-800. Therefore, both surface adsorption and pore diffusion were the two mechanisms of toluene adsorption, and the diffusion of toluene molecules in the pores was considered as the key factor that affected the adsorption rate.

Received 10th March 2020
Accepted 5th June 2020

DOI: 10.1039/d0ra02225j

rsc.li/rsc-advances

1. Introduction

Recently, increasing pollutants are being generated and emitted into the atmosphere because of rapid industrialization and urbanization in China, which has led to the deterioration of air quality. Thus, smog-like weather is being frequently experienced in most cities. In recent years, there have been many efforts by Chinese government to reduce the emission of the pollutants and improve air quality.[1] In general, the emission of the conventional pollutants such as SO_2, NO_x and dust were significantly decreased. For example, the emitted SO_2, NO_x and dust in 2014 was 19.74, 20.78 and 17.40 million tons, which was decreased to 8.75, 12.58 and 7.96 million tons in 2017. Unfortunately, volatile organic compounds (VOCs) emission has still increased. It has been reported that the anthropogenic VOC emission in 2015 was 31.12 million tons, and the estimated VOC emission in 2020 will be 41.74 million tons.[2] Moreover, parts of VOCs are toxic and carcinogenic, which harm both human health and deteriorate the ecological environment.[3] VOCs are also regarded as one of the precursors of ozone or secondary organic aerosols.[4] The Chinese government required that VOC emission in 2020 should be <28.00 million tons. Thus, the reduction or elimination of VOC emission has been a hot wave. Currently, VOC control technologies include adsorption,[5] photocatalytic degradation,[6] condensation,[7] catalytic oxidation,[8] membrane separation,[9] combustion[10] and biological degradation.[11] Among the above VOCs treatment methods, adsorption is considered as the most potential choice because of its low operation cost, high selectivity and stability, and high removal efficiency.[3]

In general, VOCs' adsorption efficiency or selectivity significantly depends on the specific surface area (BET), pore size distribution, pore volume and surface functional groups.[12] Activated carbon (AC) has been frequently used as an absorbent due to its large BET, rich porosity and high adsorption performance.[13,14] In particular, the textural properties of AC could be controlled through preparation parameters. The BET of AC always increased with the enhancement of carbonization temperature, and the high carbonization temperature promoted the formation of micropores.[15,16] The preparation methods of AC are primarily divided into pyrolysis and hydrothermal methods. In recent years, researchers are focusing on modified AC due to the requirement for the directional regulation of pore structure. Yang *et al.* agreed that the adsorption capacity of AC had a close relation with the porosity and BET due to the capillary condensation of VOCs.[17] Lillo-Ródenas *et al.* considered that toluene and benzene were first adsorbed in the micropores.[18] Moreover, the surface functional groups such as

[a]Hubei Key Laboratory for Efficient Utilization and Agglomeration of Metallurgic Mineral Resources, Wuhan University of Science and Technology, Wuhan, 430081, P. R. China. E-mail: hanjun@wust.edu.cn; zhaobo87@wust.edu.cn

[b]Hubei Provincial Industrial Safety Engineering Technology Research Center, Wuhan University of Science and Technology, Wuhan, 430081, P. R. China

† Electronic supplementary information (ESI) available. See DOI: 10.1039/d0ra02225j

Table 1 The textural properties of ACs

Sample	S_{BET}[a], $m^2\ g^{-1}$	S_{mic}[b], $m^2\ g^{-1}$	V_0[c], $cm^3\ g^{-1}$	V_t[b], $cm^3\ g^{-1}$	D_p[d], nm	N content, %
AC-500	568	508	0.295	0.260	0.520	2.75
AC-600	1123	1120	0.574	0.528	0.547	1.98
AC-700	1269	1128	0.658	0.581	0.565	1.08
AC-800	1381	1205	0.722	0.581	0.573	0.58

[a] Surface area was calculated using the BET method at $P/P_0 = 0.05$–0.30. [b] Micropore volume evaluated by the *t*-plot method. [c] Total pore volume at $P/P_0 = 0.995$. [d] Calculated by the BJH method.

carbonyl, amino and N-functionalities in the AC surface may promote the adsorption capacity of benzene and toluene[17,19] while the oxygen-containing functional groups had a negative effect on benzene and toluene adsorption.[20]

In this work, sugarcane bagasse, as a sustainable carbohydrate-rich biomass, has been selected for producing AC as the raw material. In recent years, people have used biomass materials to prepare ACs, including rice straw, walnut hulls, and corn cobs. Compared with other raw materials, the carbon content in bagasse is as high as >80%, and it has a porous fibrous structure; therefore, it is more suitable to prepare AC with a richer pore structure.[21–23] In addition, due to the rapid development of the sugar industry, the annual output of bagasse is huge without effective use. To be prepared as AC, it can both make full use of the biomass energy inside and reduce the environmental pressure. In N-doped activated carbon, N is introduced to make the prepared sample surface carry N-containing functional groups, which could change the interaction between surface electrons and toluene and thereby promote adsorption ability. Certain studies reported that nitrogen-doped activated carbon can change its surface functional groups and promote electronic interaction between activated carbon and toluene. Commonly, N-doping materials include diethylenetriamine (DEA), triethylenetetramine (TETA), tetraethylenepentamine (TEPA), melamine and pyrrole.

In this paper, a series of N-doped AC derived from sugarcane bagasse (SB) were prepared. Moreover, toluene was used as a typical VOC, and its adsorption performance and mechanism in our AC were discussed in detail.

2. Experimental

2.1 AC preparation procedure

Waste agricultural biomass (sugarcane bagasse) was carbonized to prepare AC, which was purchased from Sugarcane Industry Research Institute (Guangxi, China). The obtained raw material was first pre-treated by washing, drying, and cutting. Thus, the sample of 0.6×0.8 mm was prepared. Other chemicals such as commercial activated carbon (named AC-commercial), urea, potassium hydroxide, toluene and hydrochloric acid were provided by Sinopharm Chemical Reagent Co., Ltd.

First, the pre-treated sugarcane bagasse (SB) sample was mixed with urea at a urea/SB weight ratio of 15 wt%. Then, the distilled water was added to dissolve urea into the solution. After agitation for 12 h, the solution was dried 105 °C until water was removed. Thereafter, the dried sample was carbonized under 600 °C with nitrogen protection. After carbonization for 30 min, heating was stopped and sample was cooled by nitrogen gas to 30 °C. The carbonized SB was then collected and washed through distilled water until pH was 7.0. Finally, N-doped sample was activated with KOH (KOH/sample weight ratio was 2.0), and the activated temperature was 500, 600, 700 and 800 °C. The prepared ACs was named as AC-*x*, where *x* meant the activation temperature (°C).

2.2 Adsorption test

The adsorption tests were carried out in a quartz tube reactor, and the inner diameter and the length of the reactor were 6 mm and 35 cm, respectively. The scheme of the experimental setup is shown in Fig. S1.† The reactor was heated by electricity. Moreover, the temperatures were recorded and controlled using a thermocouple. The carrying gas was the mixture of O_2 and N_2, and O_2/N_2 ratio was maintained at 1/4 using a flowmeter. During the adsorption test, the flow rate of carrying gas was ~100 ml min^{-1}, and the reaction temperature was 30 °C. Toluene was used as a VOC in the tests and feed by a syringe pump. The initial concentration of toluene was maintained at 1000 ppm. Before the experiment, 50 mg of AC was loaded into the reactor whose height was ~2 cm. Toluene concentrations at both inlet and outlet were on-line recorded using a gas chromatograph (GC-7820, Agilent). The breakthrough curves were plotted by the toluene concentration in the effluent gas *versus* the reaction time, and the breakthrough time was defined as the time that the toluene concentration in the effluent gas was 10% of the initial toluene concentration. Moreover, the adsorption capacity was estimated using eqn (1).[24]

$$q_e = \frac{\int_0^t V \times (C_0 - C_t) \times d_t}{m} \quad (1)$$

where q_e (mg g^{-1}) is toluene adsorption capacity at equilibrium, C_0 is the initial toluene concentration (mg L^{-1}), C_t is the toluene concentration of the effluent gas at the time of t (mg L^{-1}), V is the flow rate of the carrying gas (L min^{-1}), and m is the adsorbent mass (g).

2.3 Characterization

The texture properties (pore size distribution, BET and pore volume) of the sample were characterized using a ASAP 2020

surface analyzer (Micromeritics ASAP 2020). The crystal phase was identified by an X-ray diffraction analyzer (XRD; Rigaku RINT2000), and the morphology of the samples was discovered by scanning electron microscopy (SEM; ZEISS Merlin) and transmission electron microscopy (TEM; FEI Tecnai G^2 F30). X-ray photoelectron spectroscopy (XPS, Thermo Scientific Escalab 250Xi) and diffuse reflectance infrared Fourier transform spectroscopy (FT-IR, BRUKER TENSOR II) spectra were obtained to identify the surface functionalities. Moreover, the ultimate analysis was analyzed by an Elementar instrument (Elementar vario MICRO).

3. Results and discussion

3.1 Texture properties

N_2 isothermal adsorption and pore size distribution are presented in Fig. S2† and Table 1. It was demonstrated that the nitrogen adsorption–desorption isotherm for all ACs was type I,

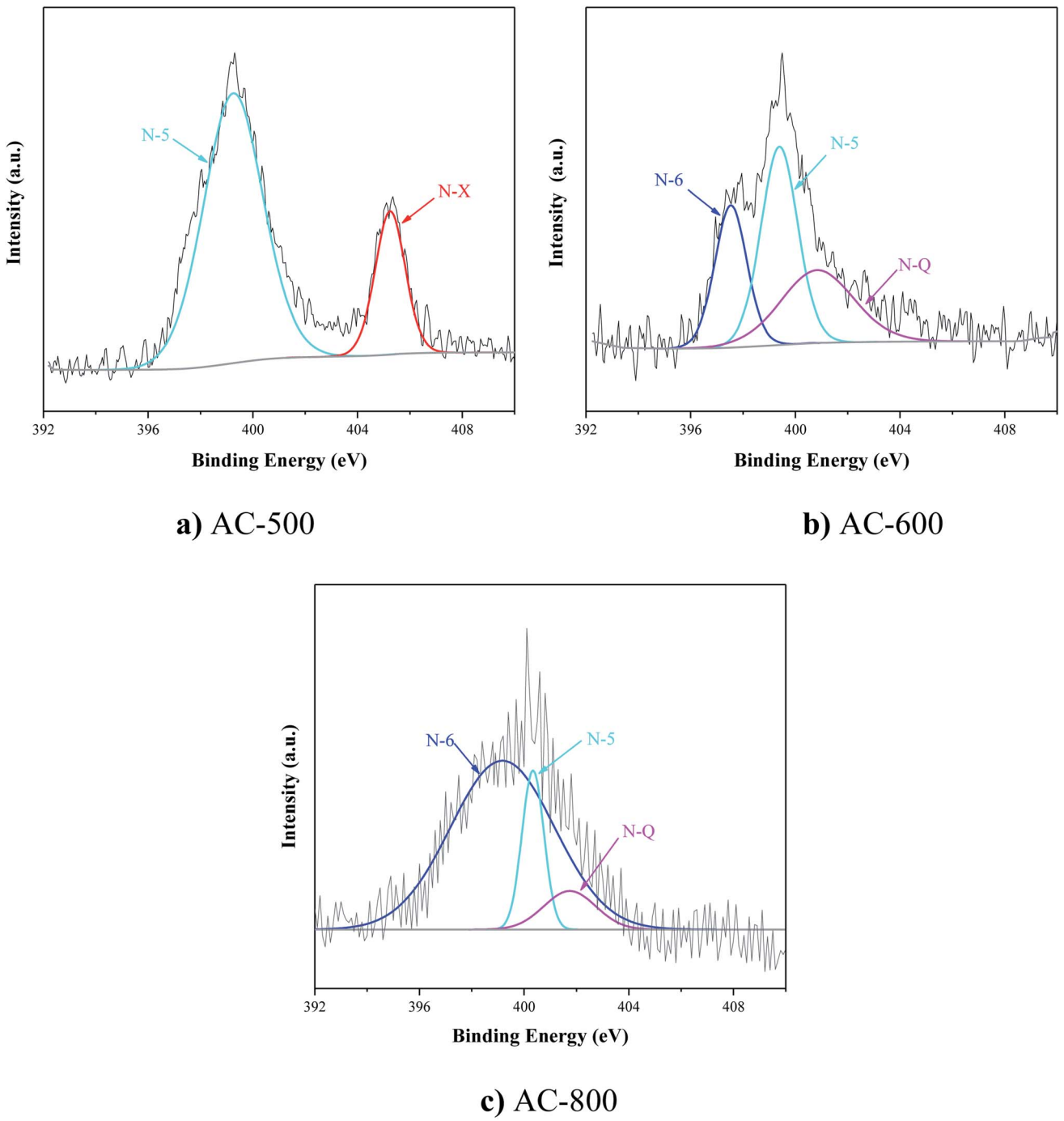

Fig. 1 N 1s XPS spectra of ACs. (a) AC-500; (b) AC-600; (c) AC-800.

and no obvious hysteresis loop was observed. Hence, it can be said that micropores are predominant. Note that AC-500 establishes its adsorption constancy at a very low relative pressure (<0.1); however, for the other samples up to $P/P_0 \approx 0.6$, which indicates that in the heat-treated samples there exist some larger pores such as supermicropores or small mesopores. Table 1 also provided detailed information of the textural properties. The BET of AC shown in Fig. S2a† sharply increased from 568 to 1123 $m^2\ g^{-1}$ when the activated temperature increased from 500 to 600 °C. The further increase of the activated temperature had a slight promotion for BET, and the BET of AC-700 and AC-800 was 1269 and 1381 $m^2\ g^{-1}$, respectively. These results may be explained by the treatment temperature being far higher to the activation temperature of KOH; therefore, the porous structure does not significantly change after heat post-treatment at higher temperatures. Due to the high energy consumption and safety risk of activation process, although further increase of activation temperature may slightly increase the specific surface area and pore volume, it is not necessary to investigate from the perspective of economy and safety in practical applications. On the basis of N_2 sorption, it can be inferred that heat treatment at different temperatures can control the porous structure of as-prepared ACs under study.

Moreover, the high activated temperature was beneficial for the total pore volume and micropore volume. In particular, the ratio of micropore volume to the total pore volume decreased from 0.88 to 0.80 when the activated temperature increased from 500 to 800 °C. The pore size distributions (PSDs) had similar tendency, as shown in Fig. S2b.† The PSDs focused on a narrow micropore diameter of <1 nm, especially 0.5–0.7 nm. Gil *et al.* believed that the micropore played a predominant role in toluene adsorption when toluene concentration was low.[25] Moreover, the presence of mesopores was in a favor of the diffusion of VOC molecules and promoted adsorption capacity.[26]

3.2 Surface functional groups

Fig. S3† and 1 show the surface functional groups identified by FTIR and XPS. In Fig. S3,† there was a broad peak at 3419 cm^{-1} assigned to C–H; its intensity increased with the enhancement of activated temperature. However, the high activated temperature had a negative effect on C–C and C–O groups located at 1560 and 1092 cm^{-1}. Yang *et al.* reported that the removal of surface oxygen-containing functional groups could promote the adsorption capacity of VOCs. The existence of oxygen groups decreased the free electron density at the carbon basal plane and suppressed the interaction between toluene and π-electron adsorbents.[27]

Moreover, the peaks of N 1s spectra at 398.1, 400.3, and 401.6 were regarded as pyridinic-N (N-6), pyrrolic-/pyridonic-N (N-5), and quaternary-N (N-Q). Fig. 1 and Table 1 reported that the increase of the activated temperature could accelerate the decomposition of N-containing functional groups and the formation of N-6 (Fig. 1b and c). The fraction of N-6 was not observed in Fig. 1a, and N-6 was the main component of N-containing functional groups in AC-800. Tehrani *et al.* reported there was an interaction between the π electron density of AC and N-containing functional groups; moreover, N-containing functional groups had an affinity for toluene, which was favorable for toluene adsorption.[34] According to the fraction of N-containing functional groups and the binding energy of toluene on N-containing functional groups,[13] pyridinic-N (N-6) contributed more to toluene adsorption for AC-800. Moreover, XPS spectra proved that there were O=C–OH, C–O, C=O, C–OH, O–C=O, and C–O–C oxygen containing functionalities on the AC-800 surface (Fig. 2).

3.3 Adsorption test

Fig. 3 shows the breakthrough curve of toluene. It shows that the breakthrough time of AC-*x* increased from 38 to 75 min when the activated temperature increased from 500 to 800 °C. Moreover, the adsorption capacity of toluene for AC-500, AC-

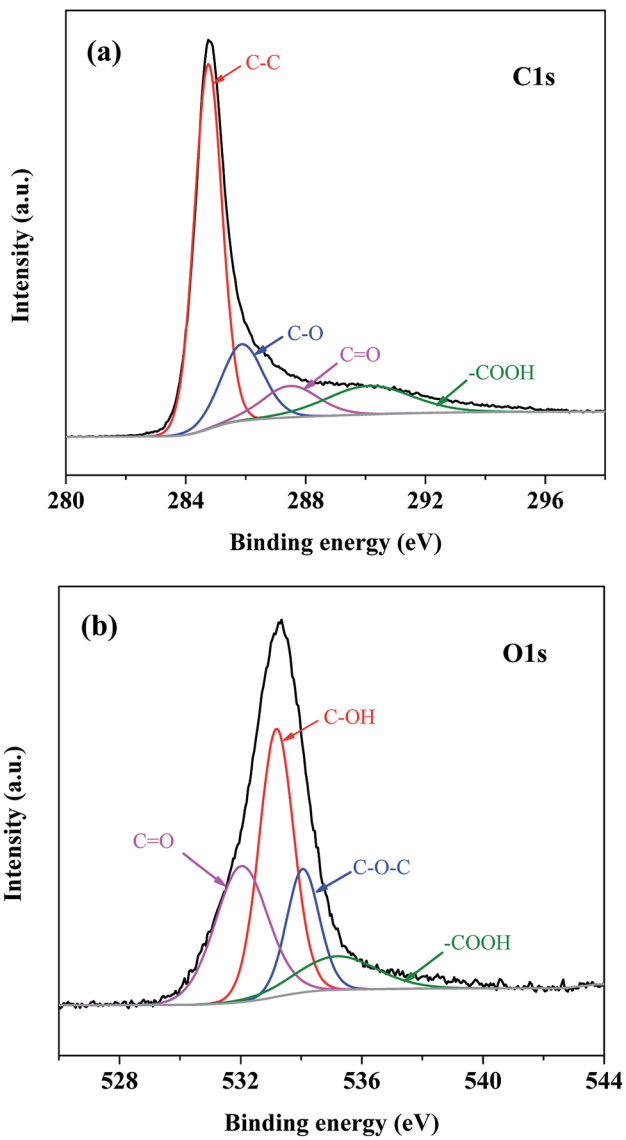

Fig. 2 (a) C 1s and (b) O 1s XPS spectra of AC-800.

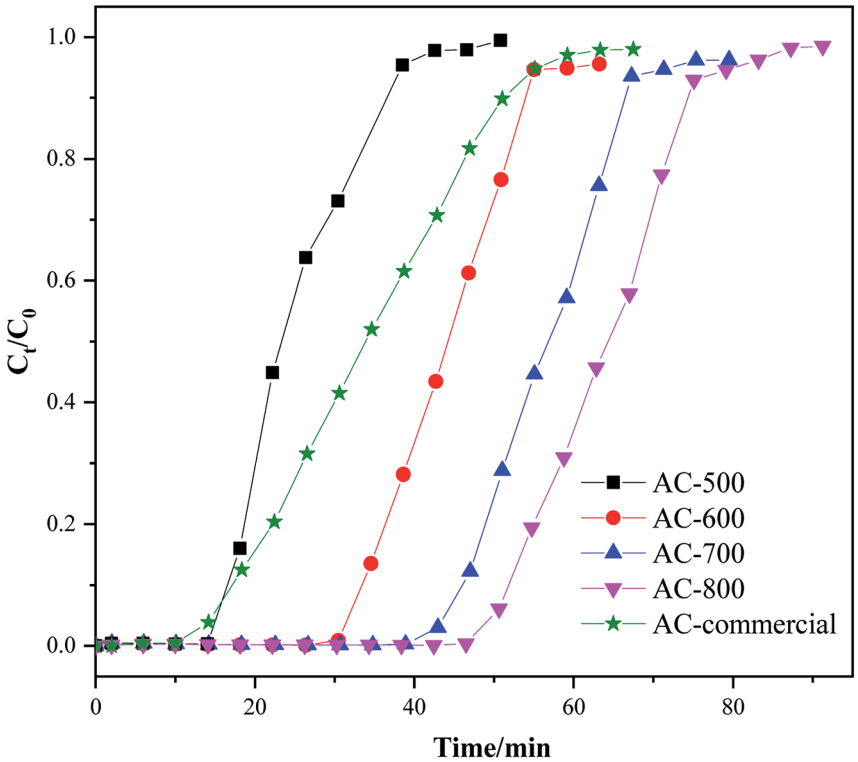

Fig. 3 Adsorption breakthrough curves of different samples.

Table 2 Toluene adsorption capacity by ACs reported in the literature

	Sorbent	Parameters	S_{BET}, $m^2\ g^{-1}$	Adsorption capacity, mg g^{-1}	Breakthrough time, min	Reference
1	Commercial AC	10.0 g m^{-3}, 50 ml min^{-1}, 298 K	934	41	100	29
2	AC/MgO	10.0 g m^{-3}, 50 ml min^{-1}, 298 K	794	56	110	29
3	AC/ZnO	10.0 g m^{-3}, 50 ml min^{-1}, 298 K	847	68	130	29
4	AC/CuO	10.0 g m^{-3}, 50 ml min^{-1}, 298 K	769	46	130	29
5	AC/ZrO_2	10.0 g m^{-3}, 50 ml min^{-1}, 298 K	837	127	120	29
6	AC derived from vegetable-tanned leather	100 ppm, 250 ml min^{-1}, 293 ± 2 K	2719	700	2500	25
7	AC derived from sewage sludge	100 ppm, 250 ml min^{-1}, 293 ± 2 K	990	350	1250	30
8	Activated biochar derived from rice husk	300 ppm, 30 ml min^{-1}, 293 K	1818	264	2784	24
9	Biochar	50 ml min^{-1}, 293 K	388	5.58–91.2		31
10	AC derived from anthracite	200 ppm, 90 ml min^{-1}, 298 K	2746	640	630	18
11	Commercial AC	150 ppm, 6 L min^{-1}, room temperature	1067	104	204	32
12	Commercial AC by acid treated	150 ppm, 6 L min^{-1}, room temperature	840	123	240	32
13	Carbon derived from coconut shell	80 ppm, 2 L min^{-1}, 303 K	1137	44	97	33
14	Commercial AC	80 ppm, 2 L min^{-1}, 303 K	1011	32	91	33
15	AC derived from corncob	3000 mg m^{-3}, 500 ml min^{-1}, 298 K	1501	414	70	26
16	AC modified with Cu	33 803 mg m^{-3}, 20 ml min^{-1}, 293 K	985.2	701.8	94	28
17	AC derived from petroleum waste	10%, 120 ml min^{-1}, 298 K	2692	659.9	65	34
18	Activated coke	190 ppm, 1000 ml min^{-1}, 298 K	534	254	25	35
19	AC derived from lignocellulosic waste	0.2 μl cm^{-3}, batch reactor, 298 K	1668	417		36
20	AC derived from lignin	400 ppm, 30 ml min^{-1}, 298 K	1513	263.4	2195	37
21	AC derived from coconut shell	250 mg L^{-1}, batch reactor, 303 K	361	357	300	38
22	AC derived from sugarcane bagasse	1000 ppm, 100 ml min^{-1}, 303 K	1381	522	86	This work

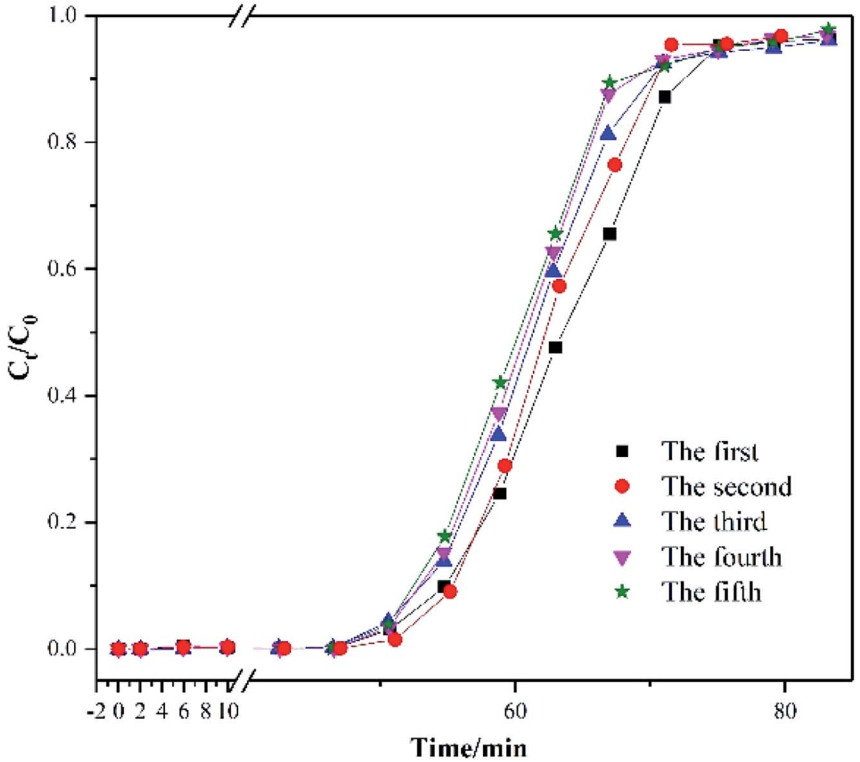

Fig. 4 The consecutive toluene adsorption–desorption cycles of AC-800.

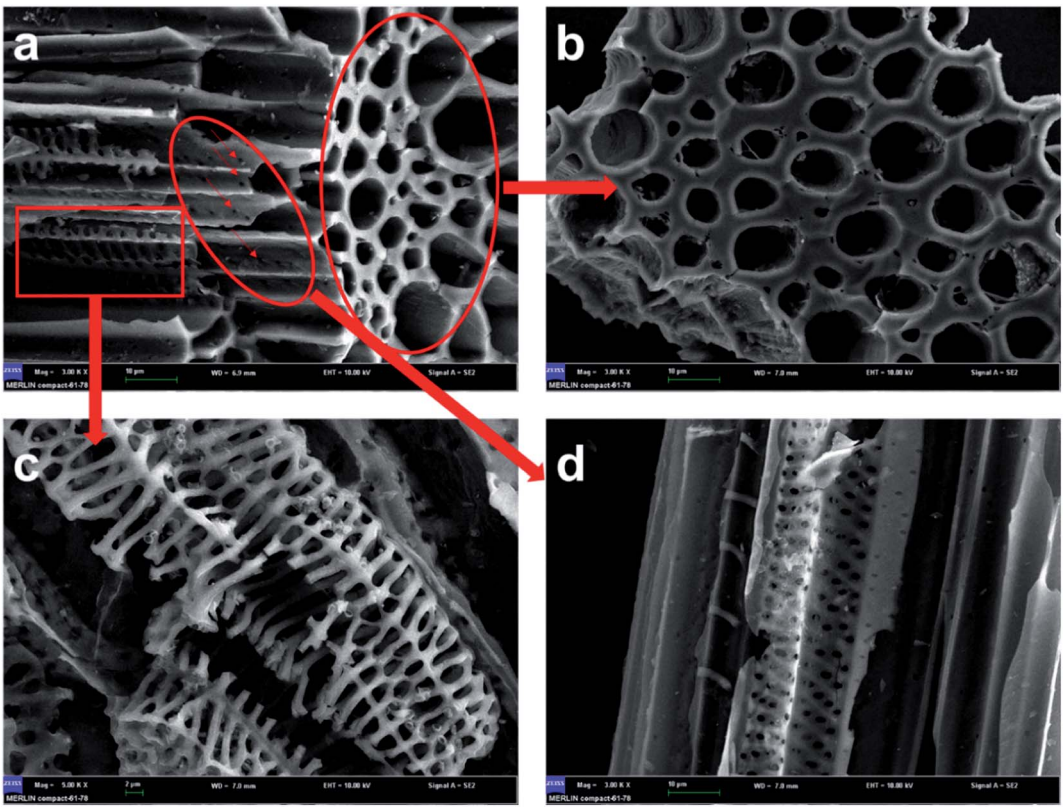

Fig. 5 (a–d) SEM images of AC-800.

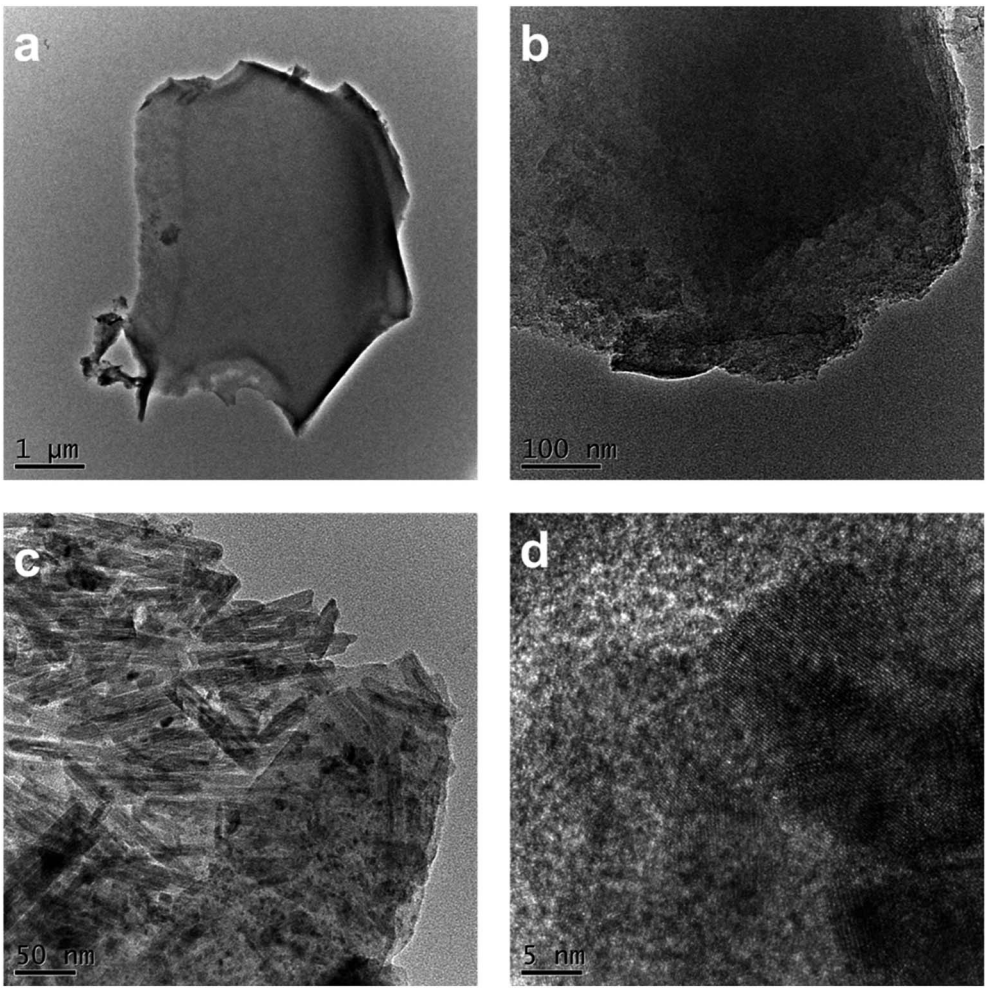

Fig. 6 (a–d) TEM images of AC-800.

600, AC-700, and AC-800 and a commercial AC derived from coconut shell was 205, 362, 462, 522, and 282 mg g^{-1}, respectively. The above results agreed with the textural properties and surface functionalities. As described in Fig. S2† and Table 1, the enhancement of the activated temperature would increase the BET and total pore volume. Moreover, the ratio of micropore volume to the total pore volume decreased. In addition, the oxygen-containing functional groups easily decomposed under the high activated temperature. Thus, the above phenomena favored toluene adsorption. Table 2 compares the toluene adsorptive capacity of our prepared AC-800 with that of other ACs in the literature. Though AC prepared by Gil,[25] Lillo-Ródenas,[18] and Lei[28] had higher toluene adsorptive capacity, the preparation of AC from the vegetable-tanned leather and petroleum waste would produce additional pollutants or increase the cost due to the addition of Cu. Moreover, the toluene adsorptive capacity of other ACs in Table 2 was lower than that of AC-800 prepared in our work.

The desorption test was carried out to understand the regeneration temperature. In this experiment, the heating rate was

Table 3 The kinetic parameters of different model

	Pseudo-first order model			Pseudo-second order model			Elovich				Bangham			
Sample	k_1/min^{-1}	R^2	q_e/mg g^{-1}	k_2/g mg^{-1} min^{-1}	R^2	q_e/mg g^{-1}	α/mg g^{-1} min^{-1}	β/mg g^{-1}	R^2	q_e/mg g^{-1}	k/min^{-1}	z	R^2	q_e/mg g^{-1}
AC-500	0.1343	0.948	207.1	9.89×10^{-5}	0.916	269.5	25.535	3.97×10^{-3}	0.967	206.6	7.57×10^{-3}	1.743	0.998	208.36
AC-600	0.0874	0.881	368.7	5.99×10^{-6}	0.723	398.4	26.871	1.10×10^{-3}	0.966	368.4	3.47×10^{-4}	2.347	0.994	364.4
AC-700	0.0737	0.869	468.9	2.69×10^{-6}	0.665	516.4	27.918	7.34×10^{-4}	0.953	470.5	1.31×10^{-4}	2.477	0.994	468.8
AC-800	0.0695	0.838	530.6	1.06×10^{-6}	0.555	557.1	28.585	6.01×10^{-4}	0.939	535.8	3.41×10^{-5}	2.760	0.991	525.3

5 °C min^{-1}. Moreover, toluene concentration of the effluent gas was analyzed by GC-7820 every 10 min. During the regeneration process, 100 ml min^{-1} nitrogen gas was fed to carry the released toluene. Fig. S4† reported that the peak of toluene concentration occurred at 130 °C. The boiling temperature of toluene was 110.6 °C. Moreover, toluene was adsorbed in the micropores, which would not vaporize unless the regeneration temperature was far higher than its boiling point. Hence, the regeneration temperature was determined as 130 °C in the cycle test. Fig. 4 shows the five consecutive toluene adsorption–desorption cycles of AC-800. The adsorption capacity of the five cycles was 522, 511, 508, 502 and 498 mg g^{-1}, which decreased by 4.5% after five cycles. The primary reduction of the adsorption capacity occurred at the first cycle. Zhang *et al.* supposed that micropore blockage and incomplete desorption was attributed to the reduction of adsorption capacity.[31] Moreover, the breakthrough time was not obviously reduced in the cycle test.

3.4 Morphology

Fig. 5 shows the SEM images of AC-800. It was observed that there were three types of structures presented in AC-800, as shown in Fig. 5a. First, there was the vascular bundle structure along the stems of SB, which meant that the texture of SB was well preserved (Fig. 5b). Second, there was a porous structure resembling a skeleton as shown in the high magnification in Fig. 5c. Furthermore, a considerable amount of worm-like micropores were found in the vascular bundle due to the activation process. These worm-like micropores can be the active sites in adsorption of VOCs, as shown in the high-magnification images (Fig. 5d).

Both TEM and HR-TEM images in Fig. 6 demonstrated the micropores were disordered and distributed. From Fig. 6a, the AC-800 existed in the form of bulky nanoparticles with diameters of ~5 μm. Because of the etching of KOH during the activation process, many cracks appeared on the block and the mesoporous structure was finally generated (Fig. 6b). Notably, the nanorod-like fibers of SB were retained after activation, which can be clearly observed in Fig. 6c. In addition to TEM images, the microstructure of AC-800 was further examined by HR-TEM in higher magnification (Fig. 6d). The gray substrate was considered as the characteristics of graphitic carbon, and the disordered fringe pattern in the sample was attributed to the amorphous carbon.[39] The XRD pattern in Fig. S5† proved that there was a broad peak at 23°, corresponding to the amorphous carbon (002), and a broad and weak peak at 43° assigned to the (100) plane of the graphitic carbon.[29,40]

3.5 Adsorption kinetics

The adsorption behavior was usually described using the kinetic model, and the adsorption mechanism was revealed through kinetic studies.[28] In this work, quasi-first-order, quasi-second-order, Elovich and Bangham kinetic models were used to fit toluene adsorption data, and the models are detail described as follows.[41,42]

(1) Pseudo-first order model

$$q_t = q_e(1 - e^{-k_1 t}) \quad (2)$$

where q_t and q_e was the amount of toluene adsorption at time t and equilibrium (mg g^{-1}), and k_1 was the quasi-second-order rate constant (min^{-1}).

(2) Pseudo-second order model

$$q_t = \frac{k_2 q_e^2 t}{1 + k_2 q_e t} \quad (3)$$

where k_2 is the quasi-second-order rate constant (min^{-1}).

(3) Elovich model

$$q_t = \frac{\ln(\alpha\beta) + \ln t}{\beta} \quad (4)$$

where α is the initial adsorption rate constant (mg g^{-1} min^{-1}) and β is the desorption rate constant (g mg^{-1}).

(4) Bangham model

$$q_t = q_e - \frac{q_e}{e^{kt^z}} \quad (5)$$

where k is the Bangham constant (min^{-1}) and z is a constant.

The parameters of the four models were summarized in Table 3. It was displayed that the correlation coefficients (R^2) were <0.99 for all the models except for the Bangham model. Moreover, the theoretical adsorption capacity of the Bangham model was closer to the experimental adsorption capacity. Hence, it can be said that the Bangham model was the best model for describing toluene adsorption in AC-800. Moreover, toluene adsorption had two mechanisms: toluene adsorption at the surface of AC and toluene diffusion in the pores;[28] moreover, toluene diffusion in the pores was the key factor affecting the adsorption rate.[43]

4. Conclusions

In this work, a series of N-doped activated carbons (AC) were prepared by carbonizing sugarcane bagasse modified with urea. Moreover, the adsorption mechanism was discussed on the basis of the experimental results and kinetic study. It was reported that BET and total pore volume increased when the activated temperature varied from 500 to 800 °C; moreover, the ratio of micropore volume to the total pore volume decreased from 0.88 to 0.80. The above results reported that the dynamic toluene adsorption capacity increased from 205 to 522 mg g^{-1}, which was better than that of ACs in the literature. The five consecutive toluene adsorption–desorption cycles proved that AC-800 was an excellent adsorbent due to its high toluene stability and well regeneration. Moreover, the Bangham model was regarded as the best model of describing toluene adsorption on AC-800. Therefore, it was deduced that the toluene adsorption had two mechanisms: surface adsorption and diffusion in the pore; furthermore, the toluene diffusion in the pores was the key factor of affecting adsorption rate.

Conflicts of interest

There are no conflicts to declare.

Acknowledgements

This work is partly founded by National Natural Science Foundation of China (Grant No. 21906125), Major Special Science and Technology Project of Hubei Province (Grant No. 2019ACA157 & 2019AHB073 & 2019ZYYD060) and Excellent Young Scientific and Technological Innovation Team of Hubei Provincial Department of Education, China (T201902).

References

1 National Bureau of Statistics, *China Statistical Yearbook*, China Statistics Press, Beijing, 2018.
2 J. Zhang, X. Chen, X. Liang, Y. Ke, L. Fan and D. Ye, Scenario analyses of the volatile organic compound emission allowance and allocation in the 13th five-year period, *Environ. Sci.*, 2018, **39**, 3544–3551.
3 M. Ouzzine, A. J. Romero-Anaya, M. A. Lillo-Ródenas and A. Linares-Solano, Spherical activated carbons for the adsorption of a real multicomponent VOC mixture, *Carbon*, 2019, **148**, 214–223.
4 G. R. Wentworth, Y.-a. Aklilu, M. S. Landis and Y.-M. Hsu, Impacts of a large boreal wildfire on ground level atmospheric concentrations of PAHs, VOCs and ozone, *Atmos. Environ.*, 2018, **178**, 19–30.
5 K. Rahbar Shamskar, A. Rashidi, P. Aberoomand Azar, M. Yousefi and S. Baniyaghoob, Synthesis of graphene by in situ catalytic chemical vapor deposition of reed as a carbon source for VOC adsorption, *Environ. Sci. Pollut. Res.*, 2019, **26**, 3643–3650.
6 W. Zou, B. Gao, Y. S. Ok and L. Dong, Integrated adsorption and photocatalytic degradation of volatile organic compounds (VOCs) using carbon-based nanocomposites: a critical review, *Chemosphere*, 2019, **218**, 845–859.
7 B. Belaissaoui, Y. Le Moullec and E. Favre, Energy efficiency of a hybrid membrane/condensation process for VOC (Volatile Organic Compounds) recovery from air: a generic approach, *Energy*, 2016, **95**, 291–302.
8 Y. Wang, D. Yang, S. Li, L. Zhang, G. Zheng and L. Guo, Layered copper manganese oxide for the efficient catalytic CO and VOCs oxidation, *Chem. Eng. J.*, 2019, **357**, 258–268.
9 S. Yi and Y. Wan, Volatile organic compounds (VOCs) recovery from aqueous solutions via pervaporation with vinyltriethoxysilane-grafted-silicalite-1/polydimethylsiloxane mixed matrix membrane, *Chem. Eng. J.*, 2017, **313**, 1639–1646.
10 M. Tomatis, M. T. Moreira, H. Xu, W. Deng, J. He and A. M. Parvez, Removal of VOCs from waste gases using various thermal oxidizers: a comparative study based on life cycle assessment and cost analysis in China, *J. Clean. Prod.*, 2019, **233**, 808–818.
11 S. Zhang, J. You, C. Kennes, Z. Cheng, J. Ye, D. Chen, J. Chen and L. Wang, Current advances of VOCs degradation by bioelectrochemical systems: a review, *Chem. Eng. J.*, 2018, **334**, 2625–2637.
12 Y. An, Q. Fu, D. Zhang, Y. Wang and Z. Tang, Performance evaluation of activated carbon with different pore sizes and functional groups for VOC adsorption by molecular simulation, *Chemosphere*, 2019, **227**, 9–16.
13 S. Cheng, Y. Qiao, J. Huang, W. Wang, Z. Wang, Y. Yu and M. Xu, Effects of Ca and Na acetates on nitrogen transformation during sewage sludge pyrolysis, *Proc. Combust. Inst.*, 2019, **37**, 2715–2722.
14 J. Han, L. Zhang, B. Zhao, L. Qin, Y. Wang and F. Xing, The N-doped activated carbon derived from sugarcane bagasse for CO_2 adsorption, *Ind. Crops Prod.*, 2019, **128**, 290–297.
15 X. Zhang, B. Gao, A. E. Creamer, C. Cao and Y. Li, Adsorption of VOCs onto engineered carbon materials: a review, *J. Hazard. Mater.*, 2017, **338**, 102–123.
16 J. Huang, Y. Qiao, X. Wei, J. Zhou, Y. Yu and M. Xu, Effect of torrefaction on steam gasification of starchy food waste, *Fuel*, 2019, **253**, 1556–1564.
17 C. Yang, G. Miao, Y. Pi, Q. Xia, J. Wu, Z. Li and J. Xiao, Abatement of various types of VOCs by adsorption/catalytic oxidation: a review, *Chem. Eng. J.*, 2019, **370**, 1128–1153.
18 M. A. Lillo-Ródenas, D. Cazorla-Amorós and A. Linares-Solano, Behaviour of activated carbons with different pore size distributions and surface oxygen groups for benzene and toluene adsorption at low concentrations, *Carbon*, 2005, **43**, 1758–1767.
19 T. García, R. Murillo, D. Cazorla-Amorós, A. M. Mastral and A. Linares-Solano, Role of the activated carbon surface chemistry in the adsorption of phenanthrene, *Carbon*, 2004, **42**, 1683–1689.
20 L. Li, S. Liu and J. Liu, Surface modification of coconut shell based activated carbon for the improvement of hydrophobic VOC removal, *J. Hazard. Mater.*, 2011, **192**, 683–690.
21 L. Chai, L. Zhang, X. Wang, L. Xu, C. Han, T.-T. Li, Y. Hu, J. Qian and S. Huang, Bottom-up synthesis of MOF-derived hollow N-doped carbon materials for enhanced ORR performance, *Carbon*, 2019, **146**, 248–256.
22 X. Wang, Z. Ma, L. Chai, L. Xu, Z. Zhu, Y. Hu, J. Qian and S. Huang, MOF derived N-doped carbon coated CoP particle/carbon nanotube composite for efficient oxygen evolution reaction, *Carbon*, 2019, **141**, 643–651.
23 J. Qian, X. Wang, L. Chai, L.-F. Liang, T.-T. Li, Y. Hu and S. Huang, Robust Cage-Based Zinc–Organic Frameworks Derived Dual-Doped Carbon Materials for Supercapacitor, *Cryst. Growth Des.*, 2018, **18**, 2358–2364.
24 Y. Shen and N. Zhang, Facile synthesis of porous carbons from silica-rich rice husk char for volatile organic compounds (VOCs) sorption, *Bioresour. Technol.*, 2019, **282**, 294–300.
25 R. R. Gil, B. Ruiz, M. S. Lozano, M. J. Martín and E. Fuente, VOCs removal by adsorption onto activated carbons from biocollagenic wastes of vegetable tanning, *Chem. Eng. J.*, 2014, **245**, 80–88.
26 J. Zhu, Y. Li, L. Xu and Z. Liu, Removal of toluene from waste gas by adsorption-desorption process using corncob-based activated carbons as adsorbents, *Ecotoxicol. Environ. Saf.*, 2018, **165**, 115–125.
27 X. Yang, H. Yi, X. Tang, S. Zhao, Z. Yang, Y. Ma, T. Feng and X. Cui, Behaviors and kinetics of toluene

adsorption-desorption on activated carbons with varying pore structure, *J. Environ. Sci.*, 2018, **67**, 104–114.

28 B. Lei, B. Liu, H. Zhang, L. Yan, H. Xie and G. Zhou, CuO-modified activated carbon for the improvement of toluene removal in air, *J. Environ. Sci.*, 2020, **88**, 122–132.

29 K. Zhou, W. Ma, Z. Zeng, X. Ma, X. Xu, Y. Guo, H. Li and L. Li, Experimental and DFT study on the adsorption of VOCs on activated carbon/metal oxides composites, *Chem. Eng. J.*, 2019, **372**, 1122–1133.

30 A. Anfruns, M. J. Martin and M. A. Montes-Morán, Removal of odourous VOCs using sludge-based adsorbents, *Chem. Eng. J.*, 2011, **166**, 1022–1031.

31 X. Zhang, B. Gao, Y. Zheng, X. Hu, A. E. Creamer, M. D. Annable and Y. Li, Biochar for volatile organic compound (VOC) removal: sorption performance and governing mechanisms, *Bioresour. Technol.*, 2017, **245**, 606–614.

32 S.-H. Pak, M.-J. Jeon and Y.-W. Jeon, Study of sulfuric acid treatment of activated carbon used to enhance mixed VOC removal, *Int. Biodeterior. Biodegrad.*, 2016, **113**, 195–200.

33 X. Zhao, X. Zeng, Y. Qin, X. Li, T. Zhu and X. Tang, An experimental and theoretical study of the adsorption removal of toluene and chlorobenzene on coconut shell derived carbon, *Chemosphere*, 2018, **206**, 285–292.

34 N. H. M. Hossein Tehrani, M. S. Alivand, A. Rashidi, K. Rahbar Shamskar, M. Samipoorgiri, M. D. Esrafili, D. Mohammady Maklavany and M. Shafiei-Alavijeh, Preparation and characterization of a new waste-derived mesoporous carbon structure for ultrahigh adsorption of benzene and toluene at ambient conditions, *J. Hazard. Mater.*, 2020, **384**, 121317.

35 Z. Qie, Z. Zhang, F. Sun, L. Wang, X. Pi, J. Gao and G. Zhao, Effect of pore hierarchy and pore size on the combined adsorption of SO_2 and toluene in activated coke, *Fuel*, 2019, **257**, 116090.

36 E. Santos-Clotas, A. Cabrera-Codony, B. Ruiz, E. Fuente and M. J. Martín, Sewage biogas efficient purification by means of lignocellulosic waste-based activated carbons, *Bioresour. Technol.*, 2019, **275**, 207–215.

37 N. Zhang and Y. Shen, One-step pyrolysis of lignin and polyvinyl chloride for synthesis of porous carbon and its application for toluene sorption, *Bioresour. Technol.*, 2019, **284**, 325–332.

38 J. Mohammed, N. S. Nasri, M. A. Ahmad Zaini, U. D. Hamza and F. N. Ani, Adsorption of benzene and toluene onto KOH activated coconut shell based carbon treated with NH_3, *Int. Biodeterior. Biodegrad.*, 2015, **102**, 245–255.

39 A. Pophali, K.-M. Lee, L. Zhang, Y.-C. Chuang, L. Ehm, M. A. Cuiffo, G. P. Halada, M. Rafailovich, N. Verma and T. Kim, First synthesis of poly(furfuryl) alcohol precursor-based porous carbon beads as an efficient adsorbent for volatile organic compounds, *Chem. Eng. J.*, 2019, **373**, 365–374.

40 X. Ma, L. Li, R. Chen, C. Wang, K. Zhou and H. Li, Porous carbon materials based on biomass for acetone adsorption: effect of surface chemistry and porous structure, *Appl. Surf. Sci.*, 2018, **459**, 657–664.

41 L. Tang, L. Li, R. Chen, C. Wang, W. Ma and X. Ma, Adsorption of acetone and isopropanol on organic acid modified activated carbons, *J. Environ. Chem. Eng.*, 2016, **4**, 2045–2051.

42 X. Zhang, B. Gao, J. Fang, W. Zou, L. Dong, C. Cao, J. Zhang, Y. Li and H. Wang, Chemically activated hydrochar as an effective adsorbent for volatile organic compounds (VOCs), *Chemosphere*, 2019, **218**, 680–686.

43 H. Gong, W. Liu, L. Liu, N. Goyal, P. Xiao, G. Li, Y. Wei and T. Du, In-situ synthesis of an excellent CO_2 capture material chabazite, *J. Taiwan Inst. Chem. Eng.*, 2019, **103**, 160–166.

